# First efforts in numerical modeling of tungsten migration in WEST with SolEdge2D-EIRENE and ERO2.0

A. Gallo<sup>a</sup>, A. Sepetys<sup>b</sup>, J. Romazanov<sup>c</sup>, Y. Marandet<sup>a</sup>, S. Brezinsek<sup>c</sup>, H. Bufferand<sup>b</sup>, G. Ciraolo<sup>b</sup>, Y. Corre<sup>b</sup>, S. Ertmer<sup>c</sup>, N. Fedorczak<sup>b</sup>, J. Gunn<sup>b</sup>, A. Kirschner<sup>c</sup>, C. Martin<sup>a</sup>, O. Meyer<sup>b</sup>, G.J. van Rooij<sup>d</sup>, P. Roubin<sup>a</sup>, E. Tsitrone<sup>b</sup>, the EUROfusion PFC team<sup>1</sup> and the WEST team<sup>2</sup>.

<sup>a</sup> Aix Marseille Univ, CNRS, PIIM, UMR 7345, Marseille F-13397, France

#### Abstract

First simulations of tungsten migration in WEST are performed with the SolEdge2D-EIRENE and ERO2.0 codes to support experimental investigations on the erosion of plasma-facing components and plasma impurity content. The impact of varying the background density on i) the amount of tungsten penetrating the confined plasma, ii) the promptly redeposited fraction, and iii) the erosion and deposition patterns on the wall is investigated under the working assumptions of a simplified toroidally symmetric wall contour, typical L-mode values of the transport coefficients, and deuterium plasma with a 1% oxygen content. The lower divertor is found to be the main zone of net tungsten erosion and deposition. This pattern is reduced at high background density due to the higher promptly redeposited fraction.

<sup>&</sup>lt;sup>b</sup>IRFM, CEA-Cadarache, F-13108 Saint-Paul-lez-Durance, France

<sup>&</sup>lt;sup>c</sup>Forschungszentrum Jülich GmbH, Institut für Energie- und Klimaforschung-Plasmaphysik, D-52425 Jülich, Germany

<sup>&</sup>lt;sup>d</sup>DIFFER - Dutch Institute for Fundamental Energy Research, De Zaale 20, 5612 AJ Eindhoven, the Netherlands

<sup>&</sup>lt;sup>1</sup>http://www.euro-fusionscipub.org/PFC

<sup>&</sup>lt;sup>2</sup>http://west.cea.fr/WESTteam

## 1 Introduction: tungsten migration in WEST

The plasma-facing components (PFCs) of tokamaks undergo severe particle bombardment by ions and neutrals: atoms can be eroded from the surface by momentum transfer (physical sputtering) or by forming chemical bonds with the projectiles (chemical sputtering, chemical erosion) [1]; eroded atoms enter the plasma, get ionized, start gyrating along magnetic field lines and undergo collisions (transport); impurities eventually reach back to the wall where they can be deposited as well as erode other atoms (redeposition). The ensemble of these three phenomena, called material migration, represents a severe issue for both lifetime and performance of the PFCs, due to material loss, degradation of thermo-mechanical properties and enhanced fuel retention in redeposited layers, as well as for the performance of the reactor as the plasma core is polluted by impurities which dilute the fuel mixture and cool the plasma through radiative losses, which are stronger for elements with a high atomic number Z. In particular, the assessment of tungsten (W) migration is mandatory due to its Z = 74 and in view of the extensive use of this material in future machines like ITER (divertor [2]) and DEMO (divertor [3] and first wall [4]). An ideal test bed is the WEST experiment [5], a new full-W tokamak capable of long pulse operations, whose main PFCs are sketched in the poloidal cut in figure 1.

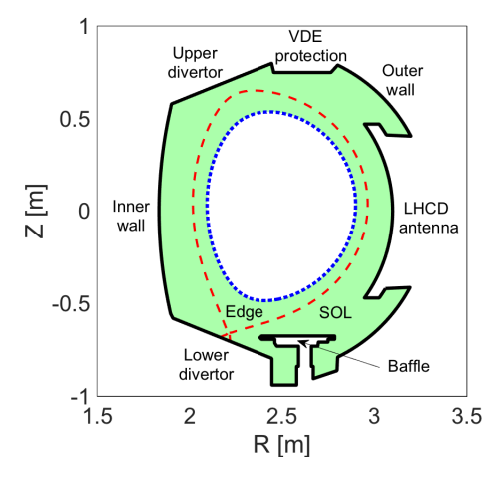


Figure 1: WEST wall contour (black solid line) with the most relevant plasma facing components, domain of the SolEdge2D-EIRENE simulation (green area), inner boundary (blue dotted line) and separatrix (red dashed line).

A number of dedicated W migration experiments are ongoing in WEST, which is equipped with visible and VUV spectroscopy, removable W samples for post-mortem analysis, erosion markers and a collector probe. All these diagnostics require the support of numerical modeling of the impurity transport for the interpretation of the experimental data. For this reason we carried out the very first simulations of W migration in WEST, by modeling the plasma background with SolEdge2D-EIRENE [6, 7], as shown in section 2, and the tracking of eroded W particles with ERO2.0 [8], as presented in section 3. Conclusions and future work are then discussed in section 4. This work fits in the broader context of W migration modeling studies, following previous investigations in DIII-D [9, 10, 11], AUG [12, 13] and JET [14, 15].

# 2 Modeling of plasma background: SolEdge2D-EIRENE

The 2D multi-fluid plasma solver SolEdge2D [6], coupled with the kinetic Monte Carlo neutral code EIRENE [7], is used to model the WEST plasma background and calculate quantities needed for modeling impurity migration: density n, electron temperature  $T_{\rm e}$ , ion temperature  $T_{\rm i}$  and parallel velocity u. In the absence of impurities, quasineutrality  $(n_e = n_i = n)$  and ambipolarity  $(u_e = u_i = u)$  are enforced. The simulation domain, indicated by the colored area in figure 1, consists of a 2D poloidal cross section of the device and extends from an inner boundary (blue dotted line), located at the edge of the confined region  $\simeq 5$  cm inside the separatrix (red dashed line), to the WEST wall contour (black solid line). The SolEdge2D-EIRENE (S2DE in the following) mesh is based on the magnetic equilibrium of plasma discharge #53711, part of the first experiment dedicated to the characterization of W sources in WEST [16]. In such equilibrium, referred to as close X-point configuration, the distance between the X-point and the lower divertor target is of  $\simeq 3$  cm. It is known that position, magnitude and shape of the top of the plasma are affected by an uncertainty that is hard to quantify at the time of writing: therefore, the plasma background in the upper divertor region, as well as the corresponding erosion patterns discussed in section 3, represent a potential source of error for this study. The main hypotheses for the presented S2DE runs are: pure deuterium (D) plasma; input power at the inner boundary  $P_{\rm in} = 1.3$  MW; outer midplane separatrix density  $n^{\rm omp} =$ 

 $5 \times 10^{18} \text{ m}^{-3}$  and  $1 \times 10^{19} \text{ m}^{-3}$ , respectively named low and high density in the following; typical L-mode transport coefficients, constant across the whole simulation domain, for particle  $D=1 \text{ m}^2\text{s}^{-1}$ , electron and ion energy  $\chi_e=\chi_i=2 \text{ m}^2\text{s}^{-1}$  and momentum  $\nu=1 \text{ m}^2\text{s}^{-1}$ ; and recycling coefficient at the full-W wall R=0.99. Despite the multi-fluid capabilities of S2DE, impurities are not modeled in these simulations as currently a single plasma background ion species is accepted as input by ERO2.0. Accounting for differences in the spatial distribution of density and temperature between the main ion and impurity ions is a crucial aspect that will be addressed in future publications. The contribution of W to radiative losses is accounted for by subtracting the core radiated power from the heating power when setting the value of  $P_{\rm in}$ .

The results in terms of plasma background profiles along the outer midplane are presented in figure 2 for both low and high density case, indicated by the blue and red lines respectively. The prescribed density values at the outer midplane separatrix are achieved through a feedback on the divertor gas puff (figure 2.a). The high density case exhibits colder ions throughout the whole scrape-off layer (SOL)(figure 2.c), whereas  $T_{\rm e}$  coincides with the low density case except for the first cm outside the separatrix (figure 2.b). The decay lengths of  $n_{\rm e}$ ,  $T_{\rm e}$ ,  $T_{\rm i}$  are in the centimetric range, which is consistent with experimental observations of L-mode plasmas.

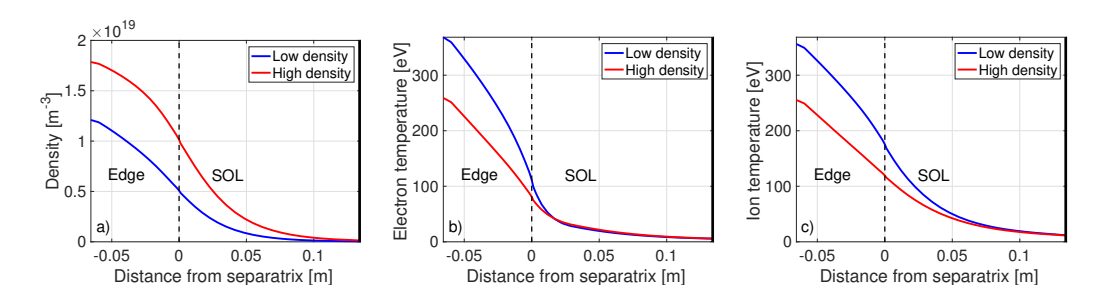


Figure 2: Background plasma profiles of a) density, b) electron temperature and c) ion temperature along the outer midplane from SolEdge2D-EIRENE runs at low (blue lines) and high density (red lines). Separatrix (black dashed line) and LHCD antenna (black solid line) radial positions.

The corresponding profiles along the wall contour are presented in figure 3. In the low density case, the peaking of the wall density  $(2-3\times10^{18}~{\rm m}^{-3})$  is

localized at lower divertor, baffle tip and upper divertor (blue line in figure 3.a). The peaking at the same locations increases by a factor  $\simeq 3.5$ ,  $\simeq 2.5$  and  $\simeq 2.4$  respectively for the high density case (red line in figure 3.a). The wall  $T_{\rm e}$ , profile, which for the low density simulation peaks at  $\simeq 70$  eV in the lower divertor, is also basically unchanged besides a  $\simeq 10$  eV reduction of the maximum value in the high density case (figure 3.b). A stronger effect of the midplane density is observed on  $T_{\rm i}$ , which in the high density case drops by  $\simeq 28$  eV,  $\simeq 22$  eV and  $\simeq 32$  eV at lower divertor, baffle and upper divertor respectively compared to the low density case (figure 3.c). The wall incident particle flux (figure 3.d), also peaks at the divertor targets and baffle tip, with a maximum value of  $\Gamma_{\rm inc} \simeq 5 \times 10^{21}$  m<sup>-2</sup>s<sup>-1</sup> and  $\simeq 10^{22}$  m<sup>-2</sup>s<sup>-1</sup> at low and high density respectively. The high  $T_{\rm e}$  and  $T_{\rm i}$  values at the wall are due to the very small radiated power in the absence of impurities,  $P_{\rm rad} \simeq 13$  kW and 37 kW for the low and high density case respectively.

Moreover, the fact that background quantities at the upper divertor have comparable values to the lower divertor and baffle ones could be an artifact due to the magnetic equilibrium reconstruction issues mentioned above. If the simulated plasma is closer to the upper divertor than in the experiment, the sharing of particle and energy flux between the two divertors could vary and with it the density and temperature profiles along these components. This could potentially impact the local erosion/deposition fluxes and therefore the global migration pattern. For all these reasons, the presented plasma backgrounds have to be regarded as test cases, not necessarily representative of the actual experimental conditions. Future work will benefit from better diagnostics coverage: for instance, a reciprocating Langmuir probe at the top of the machine will help identifying the separatrix position.

## 3 Modeling of tungsten migration: ERO2.0

The plasma backgrounds from S2DE presented in section 2 are used as input for the 3D Monte Carlo code ERO2.0 [8] which models erosion patterns and tracks eroded particles across the entire plasma volume, with full ion gyromotion resolution and accounting for all ionization states. For this very first application of ERO2.0 to WEST, the simulation domain is obtained from a simple 360° rotation of the S2DE one. Therefore, a full-W, low detail, toroidally symmetric wall is adopted. This approximation could lead to an overestimation of the W source related to the LHCD antenna (figure 1 on

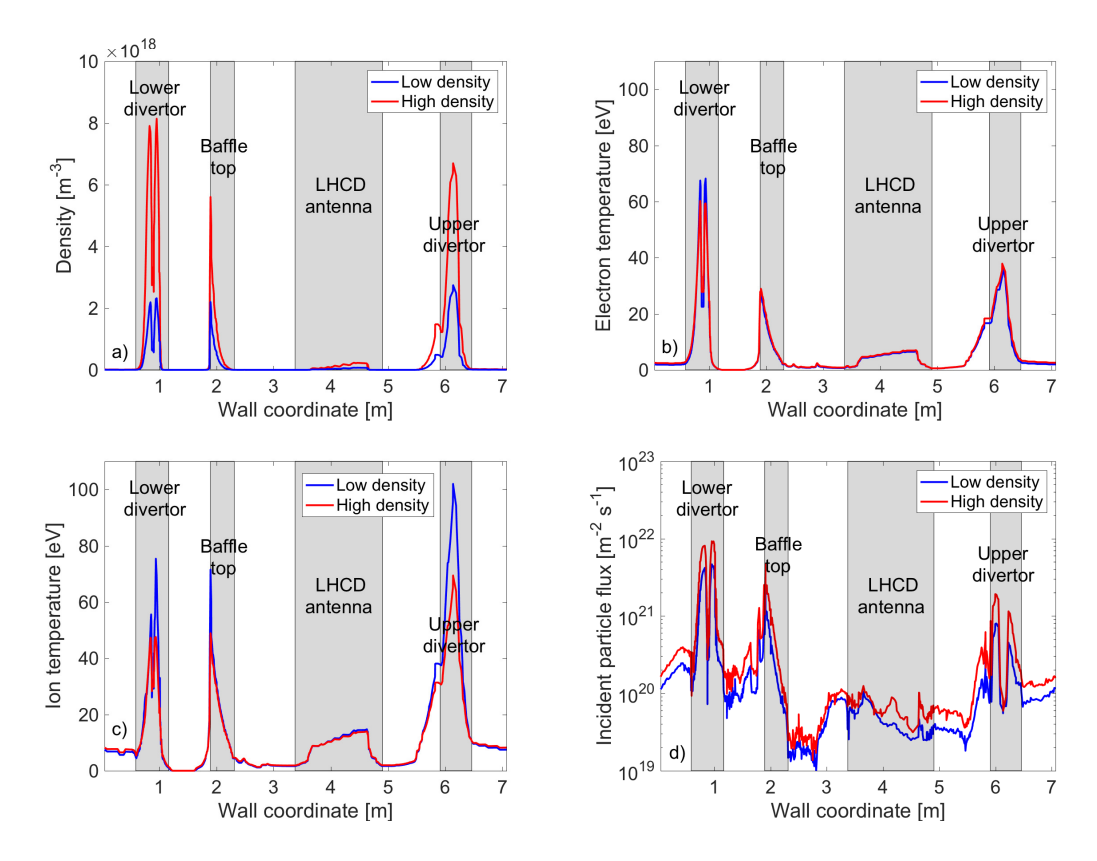


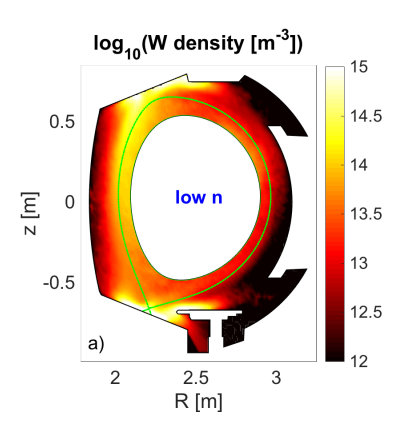
Figure 3: Background plasma profiles of a) density, b) electron temperature, c) ion temperature and d) particle flux along the wall contour from SolEdge2D-EIRENE runs at low (blues lines) and high density (red lines). Gray-shaded areas with labels indicate the location of the different PFCs.

the right), that in reality has a toroidal extension limited to  $\simeq 30^{\circ}$ . For this reason, in both S2DE and ERO2.0 simulations, the antenna is retracted with respect to its actual position in the experiment, increasing its distance from the outer midplane separatrix to  $\simeq 15$  cm. This is a strong working assumption as, in experimental scenarios with a wide SOL and small gap between the antenna and the separatrix, this component could in principle be the main W source. The other main assumptions for the presented ERO2.0 runs are: erosion due only to physical sputtering; trace approximation for the eroded W particles; constant transport coefficient  $D_{\rm W}=1~{\rm m^2 s^{-1}}$ ; collisionless magnetic sheath; reflection yields from SDTrimSP; ion incidence energy  $E_{\rm inc}=2T_{\rm i}+3ZT_{\rm e}$ ; mean ion incidence angle = 60° [17], according to analyt-

ical calculations [18] and particle-in-cell simulations [19] for divertor plasma conditions and grazing magnetic field angles; sputtering yields from TRIM [1] fitted with the corrected Eckstein formula [20]; and Thomson energy distribution and cosine angle distribution for eroded particles. Other species can be treated by ERO2.0, but all with the same temperature as the main ion and with a spatially constant concentration: within this framework, we assume a 1% oxygen (O) content in the S2DE background D plasma. A flat plasma background is assumed for the core by extrapolating the value at the inner boundary of the S2DE domain.

The first ERO2.0 results we present are the poloidal maps of the total W density  $n_{\rm W}$  (sum of all ionization states) for the low and high background density cases, shown in figure 4. In both simulations the peaking of  $n_{\rm W}$  is localized near divertors, baffle and VDE protection. In the low density case (figure 4.a), the region where  $n_{\rm W} > 10^{14}~{\rm m}^{-3}$  extends further away from the lower divertor beyond the X-point and from the upper divertor along the high field side SOL due to the longer ionization mean free path. The analysis of the trajectories shows that 35% of W particles are promptly redeposited, 44% locally redeposited and 21% undergo long range displacements. By integrating  $n_{\rm W}$  over the simulated plasma volume, one gets a total number of W particles  $N_{\rm W} = 1.04 \times 10^{15}$ . The penetration of W in the confined plasma can be quantified as the fraction of the total number of W particles found in the edge region (between the separatrix and the simulation inner boundary),  $N_{
m W}^{
m edge}/N_{
m W}=23\%$ . In the high density case (figure 4.b), the total amount of W is  $\simeq 1.8$  times lower ( $N_{\rm W} = 5.87 \times 10^{14}$ ), the poloidal distribution is similar but with a lower edge penetration ( $N_{\rm W}^{\rm edge}/N_{\rm W} = 14\%$ ). These results are consistent with the shorter trajectories of W particles (67% of prompt redeposition, 27% of local redeposition and 6% of long range displacements) due to the first ionization event happening closer to the erosion location in the denser plasma [21].

The balance between the W gross erosion, deposition and net flux along the wall contour is represented in figures 5.a and 5.b for the low and high density cases respectively. In both simulations the W gross erosion flux  $\Gamma_{\rm W}^{\rm ero}$  (red line) is of the order of  $10^{19}~{\rm m}^{-2}{\rm s}^{-1}$ , dominated by O (not shown) and localized mainly at the lower divertor, followed by the upper divertor and the baffle. The W deposition flux  $\Gamma_{\rm W}^{\rm dep}$  (green line) shows similar amplitude and pattern, consistently with the high fraction of promptly plus locally redeposited particles (79% for the low density simulation and 94% for the



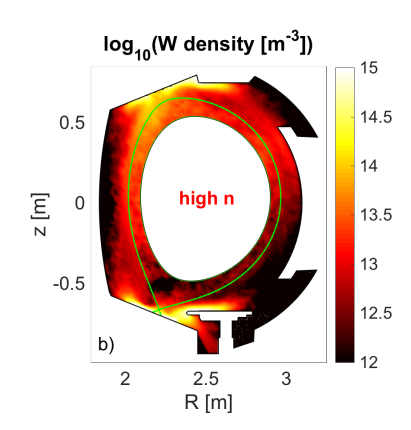


Figure 4: Maps of total tungsten density (sum of all ionization states) from ERO2.0 runs at a) low and b) high background density (1% oxygen assumed).

high density one). As a consequence, the peaking of the net W flux  $\Gamma_{\rm W}^{\rm net}$  is one order of magnitude smaller than the peaking of  $\Gamma_{\rm W}^{\rm ero}$  and  $\Gamma_{\rm W}^{\rm dep}$ . In the high density case, the peaking of  $\Gamma_{\rm W}^{\rm ero}$  and  $\Gamma_{\rm W}^{\rm dep}$  is  $\simeq 2.5$  times higher compared to the low density case despite the lower  $T_{\rm i}$  (figure 3.c), in virtue of the higher incident particle flux (3.d).

By zooming on the lower divertor region, for the low density case (figure 5.c) it is possible to detect a clear pattern in  $\Gamma_{W}^{net}$  (blue line): two net erosion zones are observed in the immediate vicinity of the magnetic strike lines, indicated by the vertical dashed black lines. These are surrounded by three deposition zones corresponding to the private flux region and inner and outer common flux regions. Such pattern is more pronounced for the outer divertor target, where  $\Gamma_{\rm W}^{\rm ero}$  is  $\simeq 30\%$  higher than at the inner divertor target due to the higher incident particle flux. These features are less obvious for the high density case (3.d) in which  $\Gamma_W^{\text{net}}$  is smaller despite the higher  $\Gamma_W^{\text{ero}}$  and  $\Gamma_W^{\text{dep}}$ . Such difference depends on the above mentioned promptly redeposited fraction of W particles (35\% for the low density case, 67\% for the high density one), allowing more local W migration in the lower divertor of the low density simulation than in the high density one. Following the approach proposed in [22], the promptly redeposited fraction observed in the presented ERO2.0 simulations is found to be in qualitative agreement with the estimate of the Fussman model [23] which, on the basis of a purely geometrical description, predicts  $\simeq 20\%$  for the low density case and  $\simeq 75\%$  for the high density one.

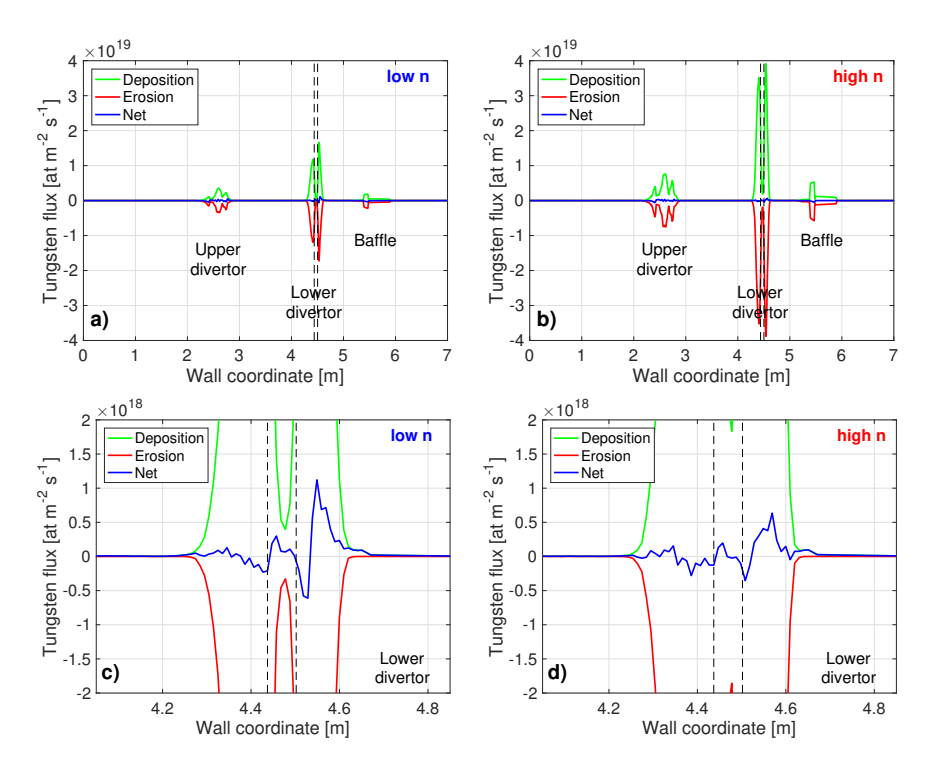


Figure 5: Tungsten gross erosion (red line), deposition (green line) and net flux (blu line) along the wall contour from ERO2.0 runs at a) low and b) high background density (1% oxygen assumed); c) and d) zoom on lower divertor. Vertical dashed black lines indicate the strike points position.

## 4 Conclusion and future work

In this contribution we showcased a first application of the modeling capabilities of SolEdge2D-EIRENE and ERO2.0 used in tandem to estimate W migration in a typical WEST discharge from the first year of operation. Due to the present scarcity of experimental data to constrain the simulations, strong working assumptions were made on input power, transport coefficients and impurity content. SolEdge2D-EIRENE pure-deuterium simulations with two different values of the outer midplane separatrix density ( $5 \times 10^{18} \text{ m}^{-3}$  and  $1 \times 10^{19} \text{ m}^{-3}$ ) provided two sets of plasma background quantities. These were used as input for ERO2.0 under the hypothesis of a spatially constant 1% concentration of O having the same temperature as D. ERO2.0 simulations highlighted lower and upper divertor, baffle and VDE protection as zones

of W gross erosion/deposition with fluxes of the order of  $\simeq 10^{19}$  m<sup>-2</sup>s<sup>-1</sup>. Increasing the background density enhanced the prompt redeposition of W (from 35% to 67%) and consequently reduced the total number of W particles in the simulation domain (from  $1.04 \times 10^{15}$  to  $5.87 \times 10^{14}$ ) as well as the penetration of W in the confined region (from 23% to 14%). In particular, the lower divertor was found to be a region of net erosion/deposition with the strike lines identified as net erosion zones and surrounded by net deposition zones in both private and common flux region. Such pattern is less pronounced at higher background density as the local redeposition of W drops (from 44% to 27%) in favour of the prompt one. Future developments of this work include: the employment of experimentally constrained plasma backgrounds; a full-detail, toroidally asymmetric wall contour; accounting for asymmetries in the poloidal distribution of light impurities; and close comparison with estimates of W gross erosion flux from visible spectroscopy.

## Acknowledgements

This work has been carried out within the framework of the EUROfusion Consortium and has received funding from the Euratom research and training programme 2014-2018 and 2019-2020 under grant agreement No 633053. The views and opinions expressed herein do not necessarily reflect those of the European Commission. Work performed under EUROfusion WP PFC.

#### References

- [1] Wolfgang Eckstein. *Sputtering Yields*, pages 33–187. Springer Berlin Heidelberg, Berlin, Heidelberg, 2007.
- [2] R.A. Pitts, S. Carpentier, F. Escourbiac, T. Hirai, V. Komarov, S. Lisgo, A.S. Kukushkin, A. Loarte, M. Merola, A. Sashala Naik, R. Mitteau, M. Sugihara, B. Bazylev, and P.C. Stangeby. A full tungsten divertor for iter: Physics issues and design status. *Journal of Nuclear Materials*, 438(Supplement):S48 S56, 2013. Proceedings of the 20th International Conference on Plasma-Surface Interactions in Controlled Fusion Devices.

- [3] J.H. You, E. Visca, Ch. Bachmann, T. Barrett, F. Crescenzi, M. Fursdon, H. Greuner, D. Guilhem, P. Languille, M. Li, S. McIntosh, A.V. Mller, J. Reiser, M. Richou, and M. Rieth. European demo divertor target: Operational requirements and material-design interface. *Nuclear Materials and Energy*, 9:171 176, 2016.
- [4] A. Del Nevo, E. Martelli, P. Agostini, P. Arena, G. Bongiov, G. Caruso, G. Di Gironimo, P.A. Di Maio, M. Eboli, R. Giammusso, F. Giannetti, A. Giovinazzi, G. Mariano, F. Moro, R. Mozzillo, A. Tassone, D. Rozzia, A. Tarallo, M. Tarantino, M. Utili, and R. Villari. Well breeding blanket design and integration for demo 2015: status and perspectives. Fusion Engineering and Design, 124:682 686, 2017. Proceedings of the 29th Symposium on Fusion Technology (SOFT-29) Prague, Czech Republic, September 5-9, 2016.
- [5] J. Bucalossi et al. this conference.
- [6] H. Bufferand, G. Ciraolo, Y. Marandet, J. Bucalossi, Ph. Ghendrih, J. Gunn, N. Mellet, P. Tamain, R. Leybros, N. Fedorczak, F. Schwander, and E. Serre. Numerical modelling for divertor design of the west device with a focus on plasmawall interactions. *Nuclear Fusion*, 55(5):053025, 2015.
- [7] D. Reiter, M. Baelmans, and P. Brner. The eirene and b2-eirene codes. Fusion Science and Technology, 47(2):172–186, 2005.
- [8] J. Romazanov, S. Brezinsek, D. Borodin, M. Groth, S. Wiesen, A. Kirschner, A. Huber, A. Widdowson, M. Airila, A. Eksaeva, I. Borodkina, and Ch. Linsmeier. Beryllium global erosion and deposition at jet-ilw simulated with ero2.0. *Nuclear Materials and Energy*, 18:331 – 338, 2019.
- [9] R. Ding, P.C. Stangeby, D.L. Rudakov, J.D. Elder, D. Tskhakaya, W.R. Wampler, A. Kirschner, A.G. McLean, H.Y. Guo, V.S. Chan, and P.B. Snyder. Simulation of gross and net erosion of high-zmaterials in the DIII-d divertor. *Nuclear Fusion*, 56(1):016021, dec 2015.
- [10] J.D. Elder, P.C. Stangeby, T. Abrams, R. Ding, A.W. Leonard, A.G. McLean, D.L. Rudakov, E.A. Unterberg, and J.G. Watkins. Oedge modeling for the planned tungsten ring experiment on diii-d. *Nuclear Mate-*

- rials and Energy, 12:755 761, 2017. Proceedings of the 22nd International Conference on Plasma Surface Interactions 2016, 22nd PSI.
- [11] X. Ma et al. this conference.
- [12] A. Geier, K. Krieger, J.D. Elder, R. Pugno, V. Rohde, and The AS-DEX Upgrade Team. Modeling of tungsten transport in the sol for sources at the central column of asdex upgrade using divimp. *Journal of Nuclear Materials*, 313-316:1216 1220, 2003. Plasma-Surface Interactions in Controlled Fusion Devices 15.
- [13] J. Karhunen, M.I. Airila, A. Hakola, A. Herrmann, M. Mayer, H.W. Mueller, R. Neu, V. Rohde, and the ASDEX Upgrade Team. Discharge-resolved erosion processes at the low-field side midplane of asdex upgrade. 39th EPS Conference and 16th Int. Congress on Plasma Physics, 2012.
- [14] Sebastijan Brezinsek, Andreas Kirschner, Matej Mayer, Aleksandra Wanda Baron-Wiechec, Irina Borodkina, Dmitriy Borodin, Ivor H Coffey, Jan Willem Coenen, Niek den Harder, Alina Eksaeva, Christophe Guillemaut, Kalle Heinola, Alexander Huber, Valentina Huber, Martin Imrisek, Stefan Jachmich, Ewa Pawelec, Stepan Krat, Gennady Sergienko, Guy Matthews, Andy Meigs, Sven Wiesen, and Anna Widdowson. Erosion, screening, and migration of tungsten in the jet divertor. Nuclear Fusion, 2019.
- [15] A. Kirschner, S. Brezinsek, A. Huber, A. Meigs, G. Sergienko, D. Tskhakaya, D. Borodin, M. Groth, S. Jachmich, J. Romazanov, S. Wiesen, and Ch. Linsmeier. Modelling of tungsten erosion and deposition in the divertor of jet-ilw in comparison to experimental findings. *Nuclear Materials and Energy*, 18:239 – 244, 2019.
- [16] G.J. van Rooij et al. this conference.
- [17] A. Kirschner, D. Matveev, D. Borodin, M. Airila, S. Brezinsek, M. Groth, S. Wiesen, A. Widdowson, J. Beal, H.G. Esser, J. Likonen, N. Bekris, and R. Ding. Modelling of the material transport and layer formation in the divertor of jet: Comparison of iter-like wall with full carbon wall conditions. *Journal of Nuclear Materials*, 463:116 – 122, 2015. PLASMA-SURFACE INTERACTIONS 21.

- [18] K. Schmid, M. Mayer, C. Adelhelm, M. Balden, and S. Lindig and. Impact of gyro-motion and sheath acceleration on the flux distribution on rough surfaces. *Nuclear Fusion*, 50(10):105004, aug 2010.
- [19] G. Kawamura, Y. Tomita, and A. Kirschner. Kinetic effects of inclined magnetic field on physical sputtering by impurity ions. *Journal of Nuclear Materials*, 438:S909 S912, 2013. Proceedings of the 20th International Conference on Plasma-Surface Interactions in Controlled Fusion Devices.
- [20] W. Eckstein. Sputtering yields. *Vacuum*, 82(9):930 934, 2008. Selected Papers from the 18th Ion Surface Interactions Conference, Zvenigorod, Russia, 24-28 August 2007.
- [21] A Kirschner, D Tskhakaya, S Brezinsek, D Borodin, J Romazanov, R Ding, A Eksaeva, and Ch Linsmeier. Modelling of plasma-wall interaction and impurity transport in fusion devices and prompt deposition of tungsten as application. *Plasma Physics and Controlled Fusion*, 60(1):014041, nov 2017.
- [22] Y. Marandet, H. Bufferand, J. Bucalossi, G. Ciraolo, S.W. Lisgo, and E. Tsitrone. Assessment of tungsten sources in the edge plasma of west. *Journal of Nuclear Materials*, 463:629 – 633, 2015. PLASMA-SURFACE INTERACTIONS 21.
- [23] G. FUSSMAN, W. ENGELHARDT, D. NAUJOKS, K. ASMUSSEN, S. DESCHKA, A. FIELD, J.C. FUCHS, C. GARCA-ROSALES, S. HIRSCH, P. IGNACZ, G. LIEDER, R. NEU, R. RADTKE, J. ROTH, and U. WENZEL. High-z elements as target materials in fusion devices. In Proc. 15th Int. Conf. on Plasma Physics and Controlled Nuclear Fusion Research (Seville), Vienna IAEA, volume 2 of LNCS. IAEA, 1995.